Weathered layer corrections

by Jan Thorbecke

4.1 Introduction

In the DELPHI project we have not yet included the influences of the unconsolidated top layer of the earth (the so called weathered layer). The disturbing influence of the weathered layer can deteriorate the result of all further data processing steps. It is therefore important to correct these influences in the surface-related pre-processing. Traditionally these corrections are called 'static' corrections, because they generally consist of time shifts applied to the seismic data. In more advanced schemes weathered layer corrections are not restricted to time shifts only, but also amplitude decay and occasionally, when detailed information about the weathered layer is available, a wave equation based correction is carried out. In the DELPHI project we are going to investigate to what extent the conventional static corrections are adequate and how an elastic wave equation based solution of the weathered layer should be implemented as part of the land data version of the pre-processing scheme.

This chapter is an introduction to weathered layer corrections. In section 4.2 a brief historical review of static corrections is given, including a short description of the existing methods. In the next section a geological view of the weathered layer is given to get some insight in the background of the geophysical problem. A simple synthetic example is worked out using upgoing incident plane waves. With this simple example we illustrate the influence of the weathered layer and investigate whether or not a time shift can correct it. Next we describe *where* in the DELPHI pre-processing scheme the static corrections should be applied and *how* the matrices for the static corrections are structured. In the last section our future plans are given.

4.2 The problem of 'statics'

The term 'statics' refers to the *wave propagation* problem of the surface layer(s) and is defined as the undesired effects in the seismic reflection data due to lateral variations in the surface layer elevation, thickness, and/or velocity. These surface layer anomalies are often divided into anomalies that have long spatial wavelengths versus those that have short spatial wavelengths (much shorter than a cable length). In solving this propagation problem three principal aspects can be distinguished:

- Estimation of the propagation parameters of the weathered layer.
- Elimination of the propagation effects.
- Transformation to a new datum.

Most weathered layer correction techniques use one effective surface layer model which takes all disturbing propagation effects of the weathered layering into account. In estimating and eliminating the weathered layer influences two different methods can be distinguished which both use this one layer model:

- The first type is a statistical method and *estimates* the related near-surface travel time anomalies (statics) and has been the subject of many papers since the earliest days of seismic exploration. The most popular estimation method is probably the linear inverse description which is first described by Taner (1974) and Wiggins (1976). This method makes use of a simple model and eliminates the weathered layer effects by a pure time shift.
- The other method makes use of a wave equation based technique to *eliminate* the effects of the weathered layer and can handle more complex weathered layer models (see for example Berryhil, 1979). But in this technique the estimation of a good weathered layer model, which is needed in the elimination process, is generally not addressed.

We will come back to those methods later in this section.

In weathered layer correction methods the effect of the near surface layer is represented by some filter. For the estimation of the parameters of this filter simplifying assumptions have been made in order to be able to reduce the number of unknowns (Taner, 1974). The two most frequent assumption made are:

Surface-consistency

Surface consistency means that a given source or receiver location on the surface is assigned with one propagation filter (see Fig. 4.1). In the most general case these propagation filters should be represented by a Greens function and surface consistency is automatically fulfilled. However, surface consistency should be enforced if simplifications are introduced.

Note that surface consistency should be replaced by source and receiver consistency if the source and receiver properties are different (in position or directivity).

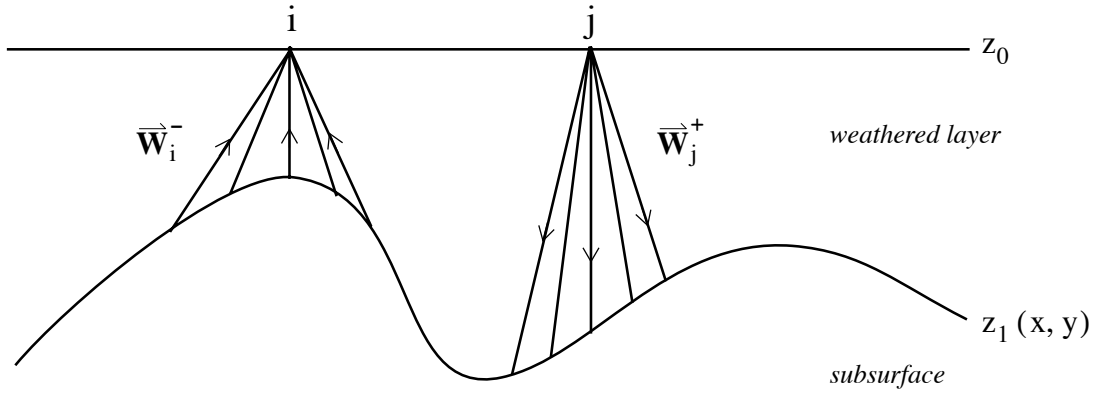

Fig. 4.1 *Surface consistency; the effects of the weathering are presented by one propagation filter per surface point.*

Time-consistency

The time-consistency assumption states that the near-surface effects do not vary with reflection time. The name "statics" is derived from this property. The time consistency assumption is only acceptable when one considers the *low velocity* of the weathered layer relative to the much higher velocities of the sub weathering layers. In the low velocity layer the waves travel along paths which are close to the vertical (see Fig. 4.2). Therefore the variation of time delay along various wave paths remains small.

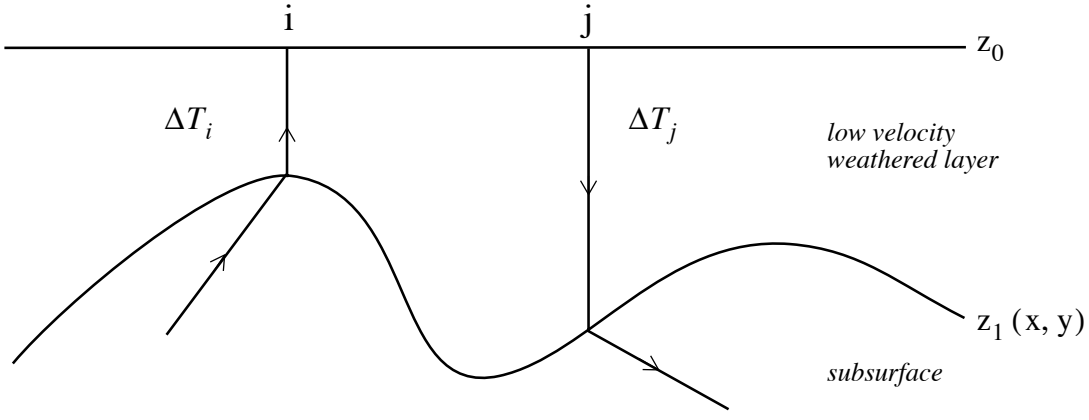

Fig. 4.2 *Time consistency; a relative low velocity weathered layer above the subsurface justifies the vertical propagation assumption.*

A consequence of both assumptions is that in the *estimation* step only *one* propagation parameter per surface point has to be calculated. And a further consequence is that *elimination* of the weathered layer effects is a pure time shift per trace regardless of the wave path.

In a convenient matrix notation these time shifts ΔT_{ij} can be notated as is indicated in equation (4.1).

$$\Delta \boldsymbol{T} = \begin{array}{c} \text{common receiver gather} \longrightarrow \\ \begin{bmatrix} \Delta T_{11} & \dots & \dots & \dots & \Delta T_{N1} \\ \dots & \dots & \dots & \dots & \dots \\ \dots & \dots & \Delta T_{ij} & \dots & \dots \\ \dots & \dots & \dots & \dots & \dots \\ \Delta T_{1M} & \dots & \dots & \dots & \Delta T_{NM} \end{bmatrix} \\ \text{common shot gather} \downarrow \end{array} \quad . \tag{4.1}$$

The total static correction for *one trace* can easily be derived from this notation and is given by

$$\Delta T_{ij} = \Delta T_i + \Delta T_j \quad . \tag{4.2}$$

Note that if $\Delta \boldsymbol{T}$ is given, an initial estimate of ΔT_i and ΔT_j can be computed; for example, an averaging procedure over one common receiver or shot gather can be carried out

$$\Delta T_i \approx \sum_{\mathrm{j}=1}^{\mathrm{N}} \frac{\Delta T_{ij}}{2\mathrm{N}} \quad , \tag{4.3a}$$

$$\Delta T_j \approx \sum_{\mathrm{i}=1}^{\mathrm{M}} \frac{\Delta T_{ij}}{2\mathrm{M}} \quad . \tag{4.3b}$$

In the next section this method will be refined.

4.2.1 Estimation of the weathered layer influences by assuming a time shift

In most static *estimation* techniques the goal is to remove the vertical travel times in the weathered layer while at the same time honoring the subweathering structures and the related normal moveout relationships. Generally, initial corrections have already been determined in the field ('field statics'), leaving the so-called residual statics. The strategies, employed for residual statics, which make use of an estimation of time delays, may be subdivided into CMP-oriented and station-oriented versions.

One of the most often used tools for the estimation of relative time shifts between traces is the cross-correlation function. The relative time delay for one trace is then the position of the largest positive peak in the cross-correlation spectrum.

The cross-correlations are made for time windows selected on the basis of estimated signal--to-noise quality. Depending on the organization of the data the cross-correlation can be computed between a reference (pilot) trace and a common shot-gather, a common receiver-gather, a common mid-point plane or a common offset plane. In our data matrix these different planes can easily be recognized (see Fig. 4.3).

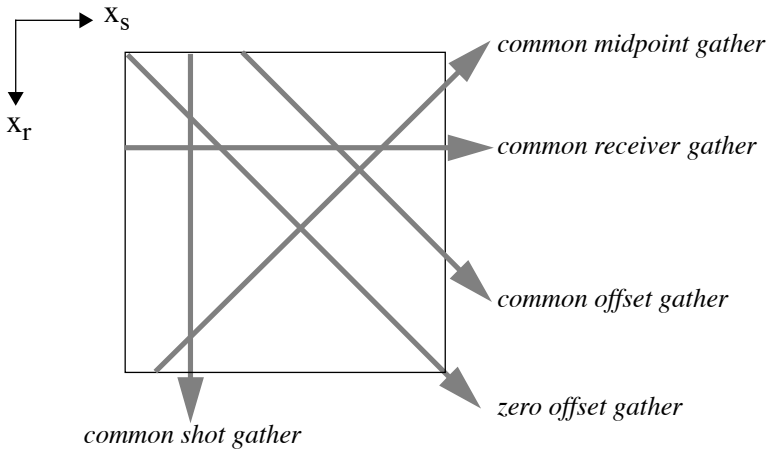

Fig. 4.3 *Different cross sections in a data matrix for one frequency component.*

The various approaches to automatic static computation differ in the way how they reduce the number of principal planes over which the time differences are computed. Taner (1974) argues that, because of the NMO delays are in general much larger than the statics, the first step to apply is a normal-moveout correction according to the best estimated velocity function. After NMO all time windows are more or less aligned in a similar manner and allows the use of fewer cross-correlation windows.

The objective of this CMP-oriented technique proposed by Taner is to compute surface consistent time shifts that yield a seismic section in which each CMP gather is aligned to produce an optimally-stacked trace. The first operation in this scheme is to obtain for each trace a time shift which aligns all primary reflections within a CMP gather. To obtain a valid static correction the sets of time shifts must be transformed, by an optimizing technique, into a set of surface-consistent (position-related) traveltimes. Following the notation of Taner, the time shift T_{ijk}, which is computed for every trace in the CMP gather is considered as a sum of several effects:

$$T_{ijk} = R_i + S_j + C_k + D_k (i - j)^2 \tag{4.4}$$

where,

R_i = receiver static at the *i*th receiver position,

S_j = source static at the *j*th receiver position,

C_k = arbritary time shift for kth CMP gather,

D_k = residual NMO component at kth CMP gather,

$(i - j)$ = source to receiver distance,

and k is the CMP position index $(k = \frac{i + j}{2})$. In comparison with equation (4.2) we see two more terms which occur due to the fact that the calculation is done in a CMP gather with residual NMO.

The offset related correction D_k stems from errors in the velocity function. Taner(1974, 1981) argues that because the offset related corrections will be in the form of spatially varying (as a function of common midpoint k) residual normal moveout the correction may be approximated by a parabola as a function of offset (which explains the $(i - j)^2$ factor in equation (4.4)).

In the approach of Taner there is one equation for each trace (source-receiver combination) in the seismic line, and there are four unknowns. The parameters R_i, S_j, C_k,and D_k given in equation (4.4) are the unknowns which, when determined, form the solution of the statics problem. Wiggins (1976) has shown that the linear simultaneous equations, that define the statics problem, are overspecified (there are more equations than unknowns) and underconstrained (they are deficient in the number of independent equations available to solve for the unknowns). Wiggins concludes further that for less than three-fold multiplicity, CMP data is inadequate to solve the statics problem.

After the calculation of the time shifts T_{ijk} the set of linear equations is solved by a linear inversion technique (for example a Gauss-Seidel process). If the CMP stack obtained with these time shifts is still not satisfactory a new velocity function for the NMO correction is calculated and new time shifts can again be obtained by cross-correlation of the traces. Wiggins(1976) gives a quantitative description of the convergence rates and the accuracy of this iterative formalism as a function of the spatial wavelength of the anomalies. For short wavelength anomalies good results are obtained with the CMP method; within a few iterations the solutions for the short wavelength anomalies are stabilized. For longer wavelength anomalies more iterations are required and the solutions have a greater uncertainty.

4.2.2 Full elimination of the weathered layer influences by assuming a known near surface model

Data transfer to a reference datum using static corrections, thus by time-shifting every seismic trace independently and assuming vertical propagation through the weathered layer, is sufficiently accurate in cases of low weathering velocities and a thin replacement layer. In other cases a more exact method, such as a data extrapolation technique based on the wave equation, should be used. The limitations of the static shift method have been studied by Shtivelman (1988) and Berryhill (1979) and are further explained in section 4.4 of this chapter.

The main problem in using wave-equation based weathered layer corrections is the determination of an accurate weathered layer model. If an accurate weathered layer model is available

then a total compensation for the weathered layer effects could be accomplished during the datum correction of standard processing. In the pre-processing part of the DELPHI project we want to investigate which method can make an effective estimation of the propagation parameters of the weathered layer.

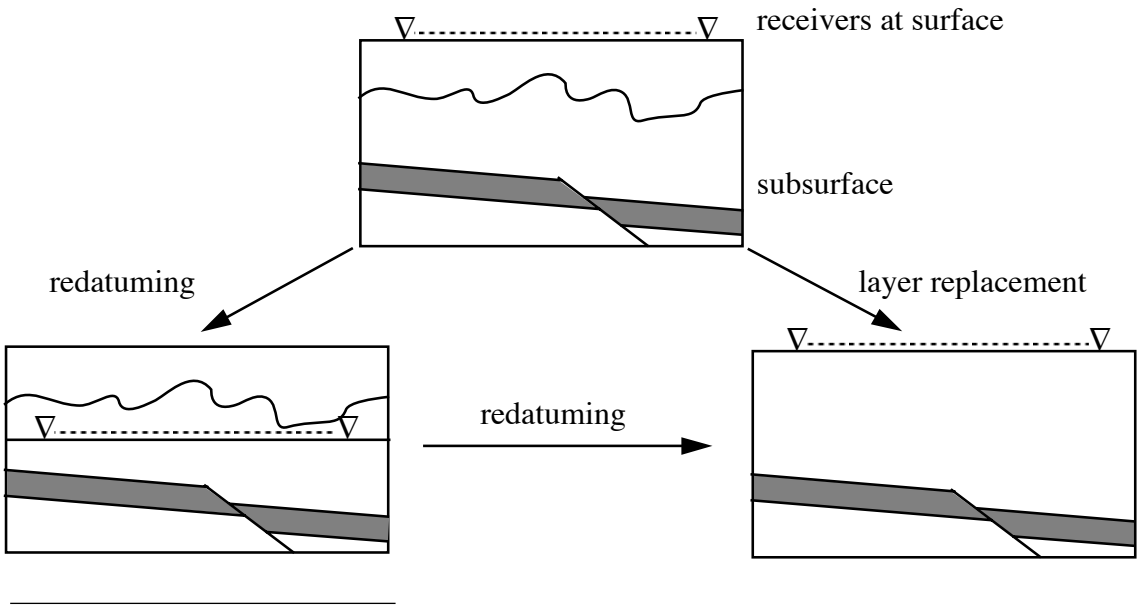

Fig. 4.4 *a) Correction of the weathered layer by layer replacement.*

The correction of the weathered layer by a wave equation based technique should be a *layer replacement* technique (Berryhill, 1979, Wapenaar and Berkhout, 1985, Yilmaz and Lucas, 1986) in which the overburden velocity is replaced with the velocity of the substratum (see Fig. 4.4) and a new datum may be chosen.

4.2.3 Conclusions

In conclusion we can distinguish three different situations and suitable solutions, which depend on the structure of the weathered layer;

- 1 - The weathered layer has very slow lateral variations. This makes the surface layer problem part of the hyperbolic NMO problem.

- 2 - The weathered layer has fast lateral variations and a very low velocity compared with the velocity of the consolidated layers. In this situation the surface layer problem is a statistical problem.

- 3 - In all other situations the thickness and velocity of the weathered layer must be estimated and a full wave theory based process must be carried out.

4.3 The weathered layer, a geological view

Weathering is geologically defined as the chemical decay and physical fragmentation, under the conditions of the earth's surface, of minerals that are formed at high pressures and temperatures in the interior of the earth. The breakdown of rock masses to fragments, ranging from bolders to clay, is the result of *chemical* wheatering combined with the forces of *physical* disintegration. The intensity of the weathering process depends upon climate, the original composition of the rock and time. The weathering process results in different clays, all types of soil and the dissolved substances that are carried away by the rivers to the ocean. Sedimentation of the fragments is the final stage of the combined process which begins with erosion and transportation of the rock fragments. The mineral content of the sediments and the structure of the sedimentation is an important factor which characterizes the top layers of the earth. In the first part of this section we will describe a general *soil profile* and in the second part the most common *structural* types of weathered layers are treated.

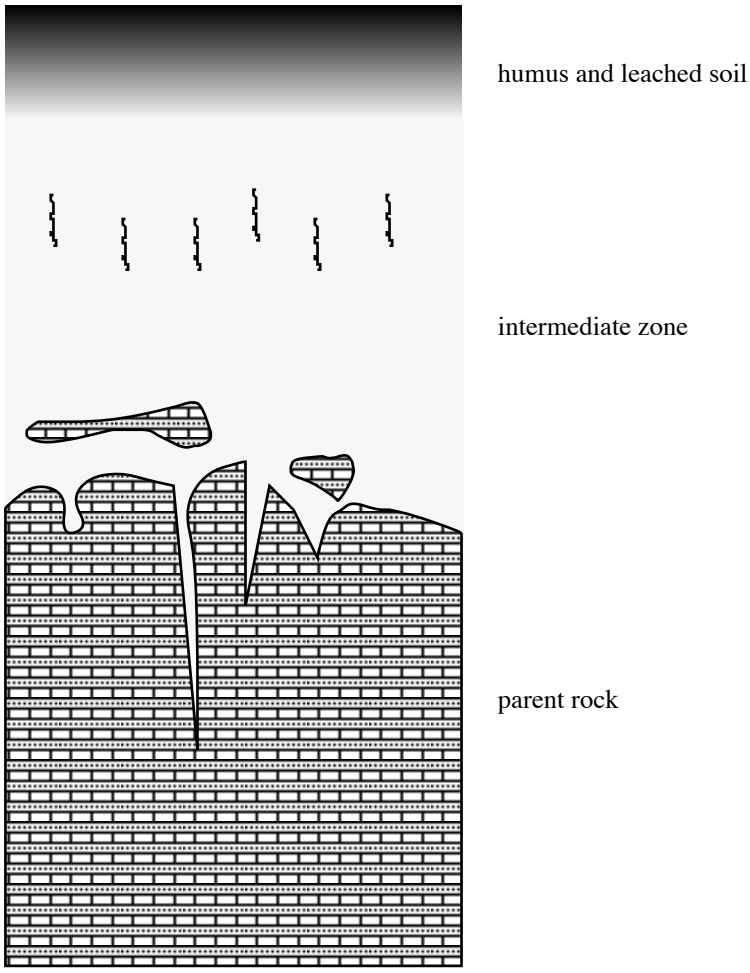

Fig. 4.5 *Profile of a typical weathered layer*

4.3.1 Soil profiles

Soil can be pictured as a thin layer that rests on bedrock (Press and Siever, 1982). A soil profile can be subdivided into three main sections. The top section contains most of the organic matter and is a zone of intense biological activity. The lowest section is slightly altered bedrock which is broken, decayed and mixed with clay. The base of this lowest section merges into the solid bedrock. Between the top and the base section there is an gradual intermediate level which contains some rock fragments and dissolved minerals from the top section. The interval depth of the three sections can vary from several meters to a thickness of 100 meter.

Fig. 4.5 shows that the top layer of the earth is very complex, anisotropic, inhomogeneous and that the interface between the weathered layer and the bedrock is not pronounced but more gradual. The characteristics of the profile are a function of the climate and the structure of the bedrock. It is known that rainfall and temperature both affect the soil formation. For example the tropics have a red soil, consisting of mostly aluminium and iron oxides and in which all silicates and carbonates are completely leached out due to the intensive rainfall.

4.3.2 Structure of the weathered layer

The geological structure of the weathered layer can be divided into four main groups which have there own specific characteristics. This division is mainly based on the occurrence of weathered layer models in recent papers.

The most simple structure is the layered structure (see Fig. 4.6a). The layers in this structure have different P- and S-wave velocities and densities. An abrupt change in the P-wave velocity can occur due to presence of a water-table. Typical values for the P-wave velocity are ranging from 600-2000 m/s, and between 200-800 m/s for the S-wave velocity (see the end of this section for a further description of the different P- and S-velocities in consolidated and unconsolidated sediments).

The second main structural group is where a dipping layer is closing into the free surface (see Fig. 4.6b). The effects of a dipping layer are much more disturbing in the seismic section than the layered model (see the example worked out in section 4.4, which uses a dipping layer model).

The third group is where the weathered layer has an irregular base level. These irregularities can originate from faults, ‘horst and graben’ tectonic, and decay of bedrock (see Fig. 4.6c). For example in an area where the bedrock consists of chalk the top layer can have a very complex structure due to the dissolving of the chalk. Beside an irregular base level the free surface level can also be laterally varying.

The fourth group, presented in Fig. 4.6d, is a top-layer which has an intrusion in it. The intrusion can for example be a bolder, an abounded river channel filled with clay, an organic mass of humus or an empty hole due to dissolving of the rock. The effects of these irregularities are very difficult to recognize in the seismic section because they occur very local (within an geo-

phone array group) and they cannot be estimated by using the conventional static estimation method. Only a special measurement, which is carried out to detect these irregularities, can give some insight in the occurrence of these intrusions.

In most practical cases a combination of the four structural elements is present in the 'real' weathered layer. For example the soil profile described in section 4.3.1 is built up from a layered, irregular and intrusion structure.

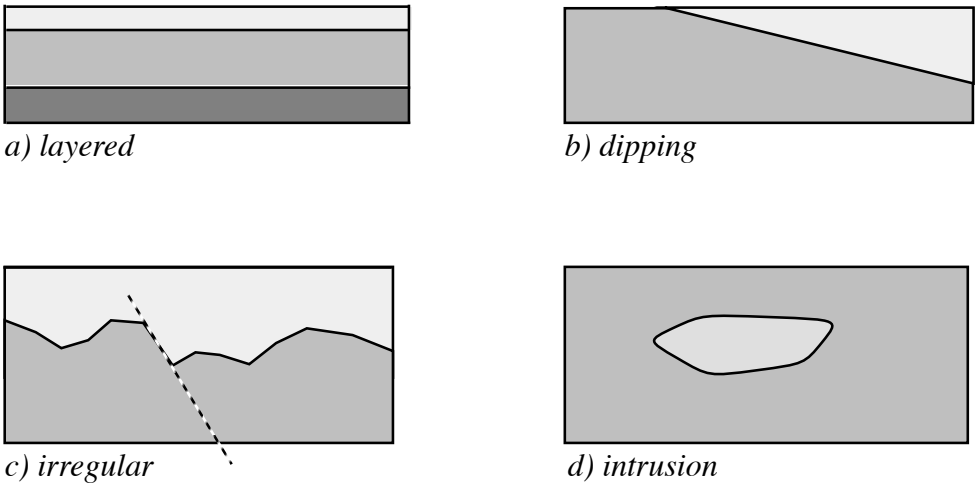

Fig. 4.6 *The four main structures of the weathered layer*

In an article of Wiest and Edelmann (1984) a comparison is made of first-arrival plots from P- and S-wave surveys of the same line measured in areas of unconsolidated sediments. The observed ratio of P- and S-wave velocities is about two for consolidated sediments. In unconsolidated near-surface layers the velocity ratio *Cp/Cs* is much larger and ratios between four and eight have been observed.

Accurate static corrections require reliable information about the near surface velocities. However, because the ratio *Cp/Cs* is very variable in the near surface, shear wave velocities have to be separately measured from the P-wave velocity. In Fig. 4.7 a comparison between P- and S-wave models, which are typical for unconsolidated sediments, is made (Wiest and Edelman 1984). For P-waves a two layer model can often be assumed. The P-wave model shows a marked velocity increase from about 600 *m/s* to 1700-1900 *m/s*. This sudden increase of the P-wave velocities is due to the stabilization at the water table. The water table can therefore be used as a reliable correction level for P-waves. In the consolidated sediments the P- wave velocities are ranging from 2000-2600 *m/s*. For S-waves a more complex vertical sequence of velocities is observed ranging from 100 to 400 m/s in unconsolidated sediments, up to 400-1200 m/s in consolidated sediments. Choosing a reliable correction level for the S-waves is more difficult

because the S-wave velocities are not stabilized at the water table and they show a slowly increasing velocity profile due to the increasing compaction and consolidation.

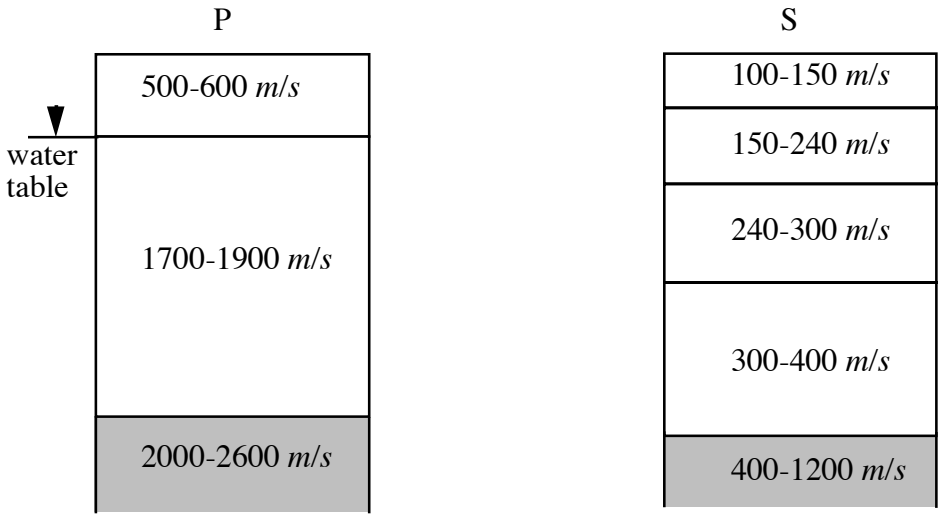

Fig. 4.7 *P- and S-wave models in unconsolidated and consolidated (shaded area) sediments*

4.4 Plane wave experiments

Some simple 2-Dimensional plane-wave experiments have been carried out to get a better understanding of what the influence is of a shallow low velocity layer on the data. We have started with a simple model which is a combination of the layered and dipping structure described in the previous section (see Fig. 4.8). The receivers in this model are positioned in such a way that one fourth of the total number of receivers is placed above the nondipping part of the model. The distance between the receivers is 2 meter and the time sampling is chosen at 1 ms.

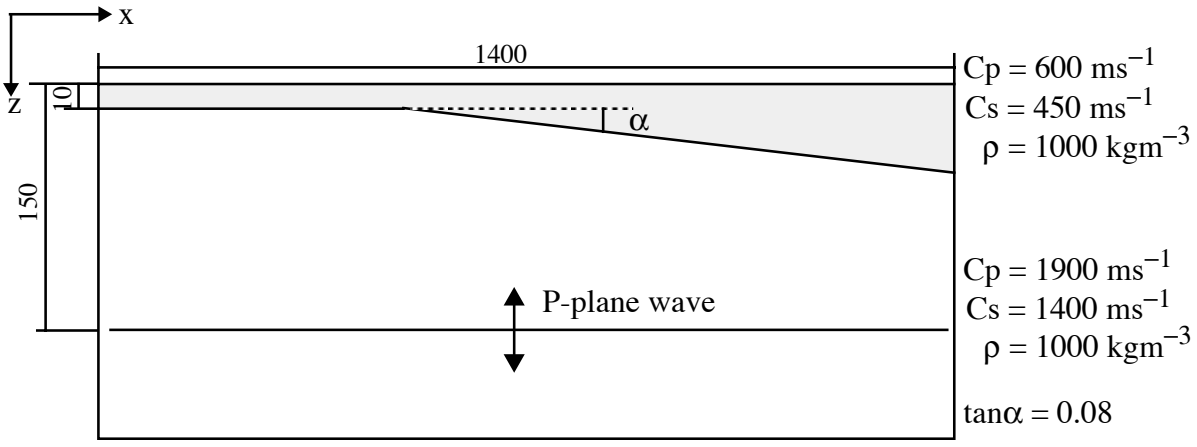

Fig. 4.8 *Subsurface model of the plane wave experiments*

An elastic finite difference program is used to obtain the snapshots and seismograms. At 150 meter below the surface an upgoing plane P-wave is emitted. The experiment is repeated for three different angles of the incident plane wave; a horizontal plane wave, a plane wave with the same angle as the dipping layer in the model, which is 4.6^{o} and a plane wave with a much higher angle of 20^{o}. The experiment with the horizontal plane wave is repeated with a different subsurface model in which the interface between the weathered layer and the lower layer is replaced by a gradual changing zone of velocity.

The time behavior and the amplitude spectrum of the Ricker wavelet we used in the experiments is shown in Fig. 4.9.

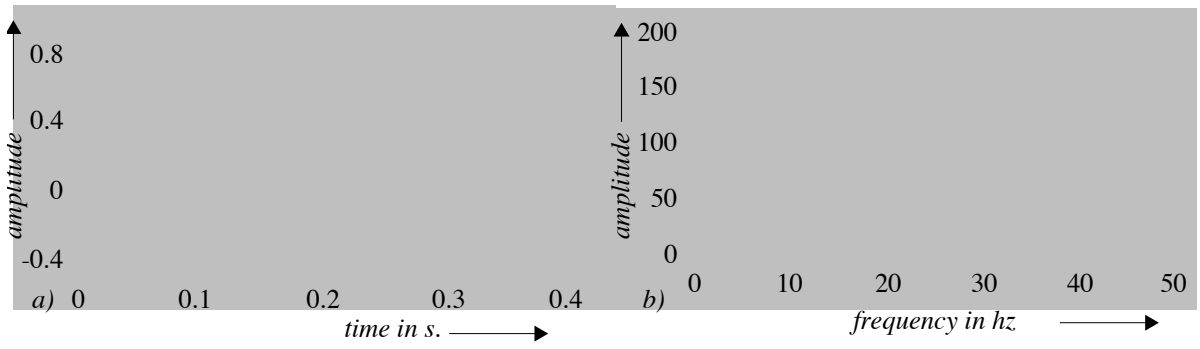

Fig. 4.9 *a) Time behavior and b) Amplitude spectrum of the wavelet used in the experiments.*

In Fig. 4.10 the vertical and horizontal component (Uz and Ux) of the received data at the surface are shown for the experiment with the horizontal plane wave. The time shifting effect of the weathered layer can be clearly seen in that part of the receivers which have their positions above the dipping layer. This effect can be seen more pronounced in Fig. 4.11 which shows the seismograms for the model with the gradual changing interface. To construct the gradual interface we have used a model with 27 small layers, with an interval depth of 2 meters, which are given a linear increase in velocity. It was necessary to construct this, maybe unrealistic, relative large interface because the average wavelength of the lower layer is about 60 meters. If we compare Fig. 4.10 with Fig. 4.11 we can see that in the experiment with the gradual interface the reflections due to the interface are nearly absent. In Fig. 4.10b the free surface multiple reflections have for higher multiples a bigger amplitude because the angle of incidence becomes with every reflection higher and gives therefore a greater contribution in the Ux displacement. In Fig. 4.11b we see that the first arrival of the plane wave is the strongest event in the record and that the free surface multiple reflections are *much* weaker than in Fig. 4.10b if we also take into consideration the higher angle of incidence for higher multiples.

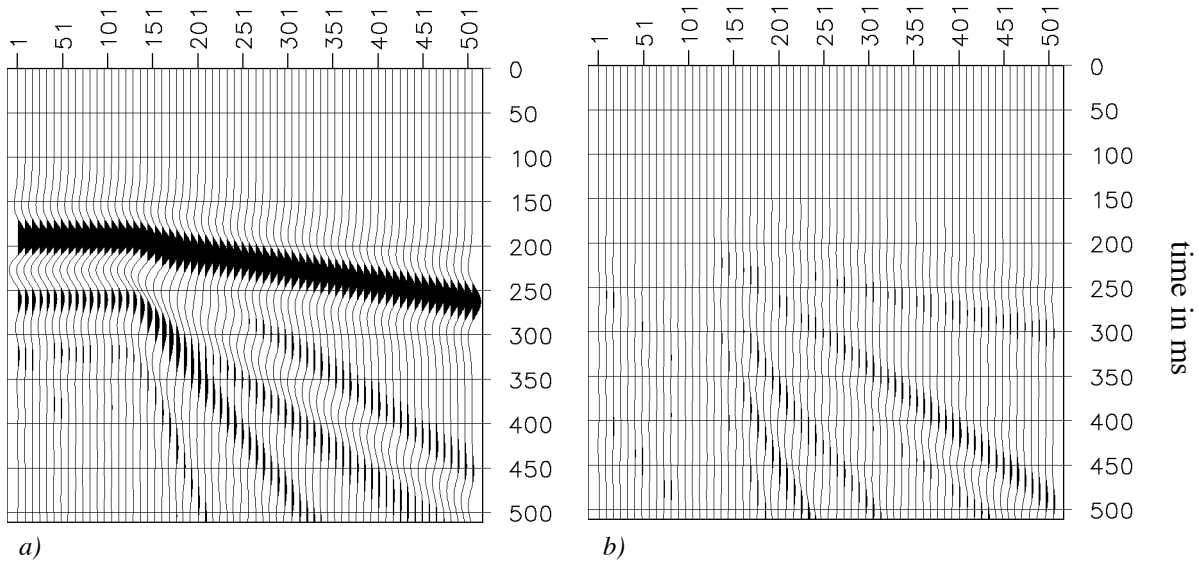

Fig. 4.10 *a) Uz-displacement and b) Ux displacement for the horizontal plane wave response in the interface model of Fig. 4.8. Note that the sections are plotted to the same amplitude.*

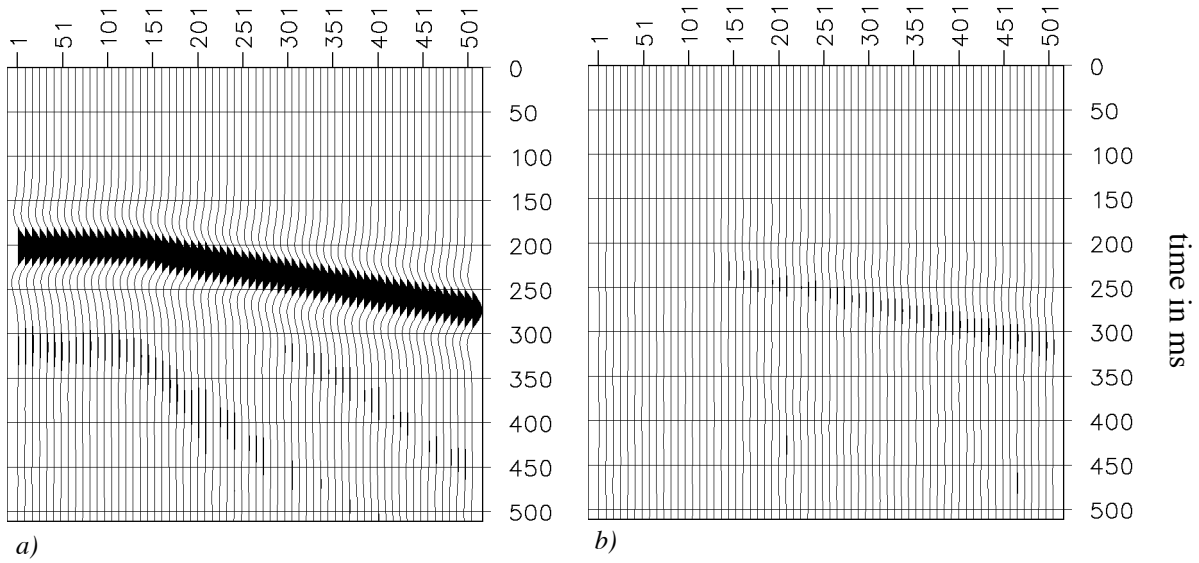

Fig. 4.11 *a) Uz-displacement and b) Ux displacement for an horizontal incident plane wave. The subsurface model has an gradual interface in comparison with Fig. 4.8. Note that the sections are plotted to the same amplitude.*

In Fig. 4.12 the Uz and Ux displacement are shown for the second experiment with the incident angle of the plane wave equal to the dipping angle of the wedge in the model. In these pictures the influence of the tilting plane wave is combined with the dipping layer in the model.

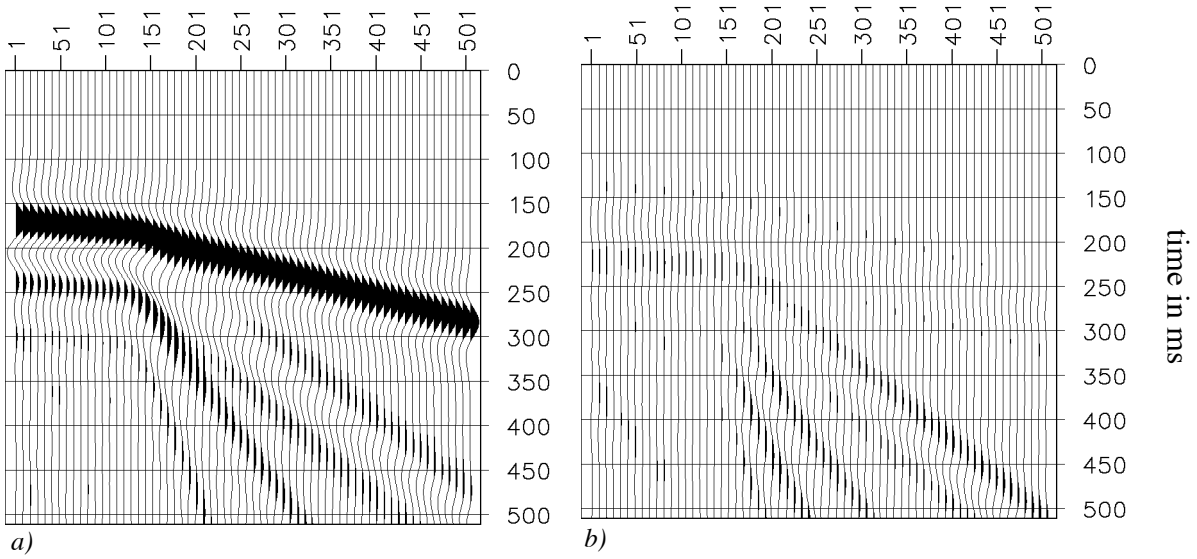

Fig. 4.12 *a) Uz-displacement and b) Ux displacement response for a plane wave with an angle of incidence of 4.6^o in the interface model of Fig. 4.8. Note that the sections are plotted to the same maximum amplitude.*

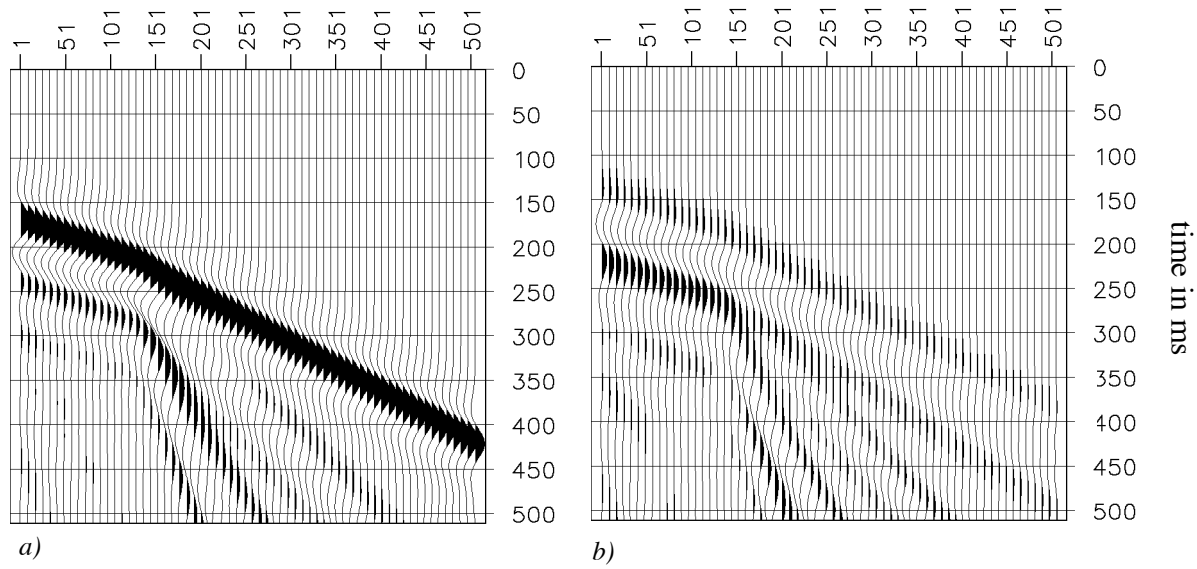

Fig. 4.13 *a) Uz-displacement and b) Ux displacement response for a plane wave with an angle of incidence of 20^o in the interface model of Fig. 4.8. Note that the sections are plotted to the same maximum amplitude.*

Fig. 4.13 shows the Uz and Ux displacements for an incident plane wave with an angle of 20^o. This experiment is done to get an impression of the reliability of the vertical assumption made in static corrections. Note that in the left hand side of all the Ux-receiver pictures the boundary artifacts of the finite difference program can be seen, these artifacts are not effects of the weathered layer.

Snapshots of the displacement in the x- and z-direction, for the horizontal plane wave, are shown in Fig. 4.14. From these snapshots it can be seen that much of the energy of the plane wave remains trapped in the low-velocity layer. This is due to the strong reflection at the interface. In Fig. 4.15 the snapshots for the vertical and horizontal component of the experiment with the plane wave of 20^o are shown.

In the snapshots of Fig. 4.14 and Fig. 4.15 different events can be observed. In the Ux-displacement snapshots the edge effects caused by the discrete plane wave, which is constructed from individual sources, can be seen as circular events in the left and right margins of the snapshots (these artifacts are indicated by arrow number 1). The downgoing wave field of the plane wave source is indicated by arrow 2. The downgoing reflection of the upgoing plane wave from the weathered layer interface is indicated by arrow 3. In a more realistic model this reflection should be very weak due to the transition zone between the weathered layer and the consolidated layers below. The first free surface reflection is indicated by arrow 4. Arrow 5 indicates free surface multiple reflections. These reflections are also much weaker in a more realistic model. Arrow 6 indicates a combination of the edge effects of the plane wave and the reflection from the free surface of this effect.

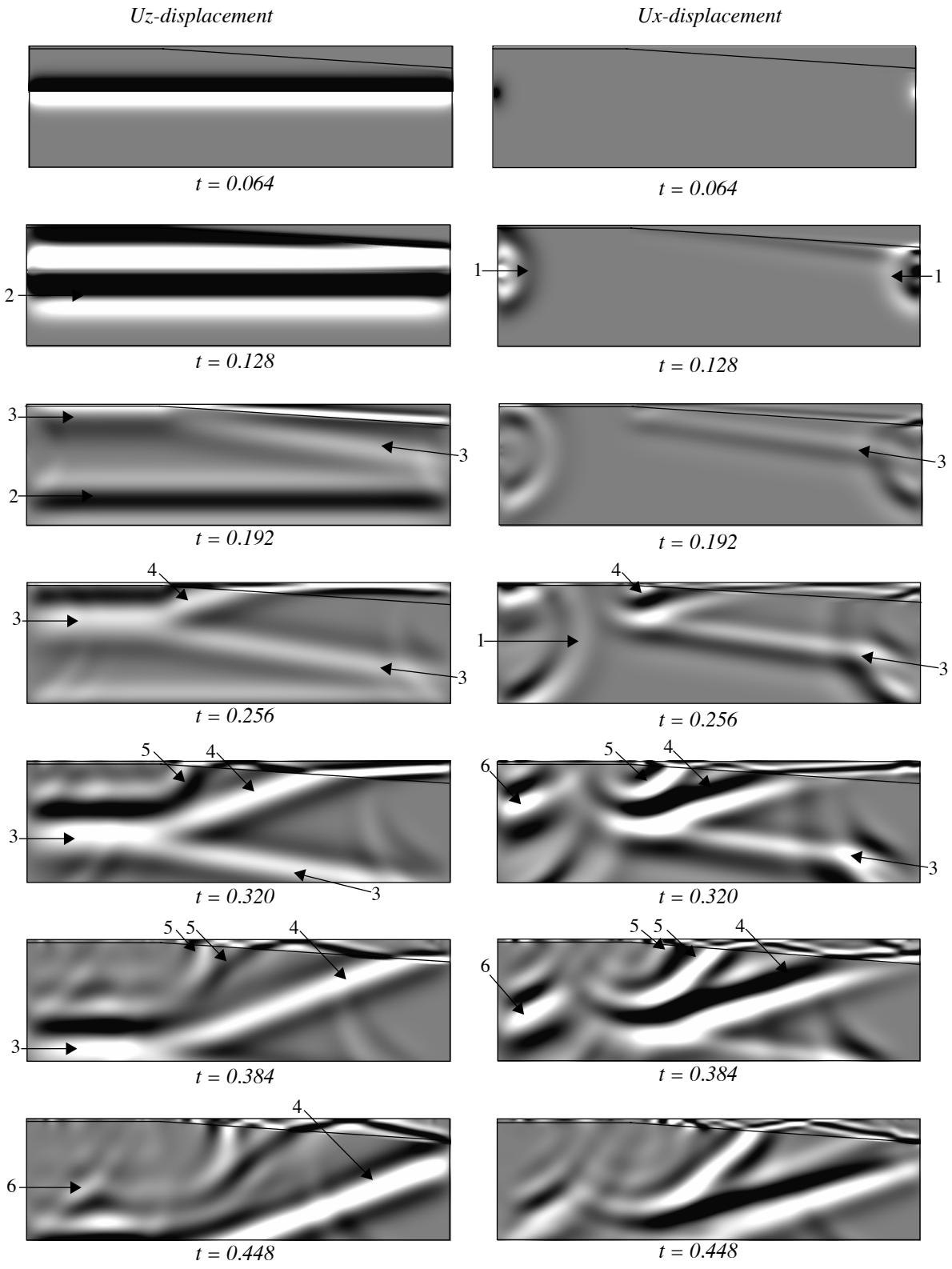

Fig. 4.14 *Snapshots of the z and x-component of subsurface model of Fig. 4.8 with an incident P- wave. The angle of incidence is 0 degrees. The snapshot interval is 0.064 seconds (the arrows are explained in the text).*

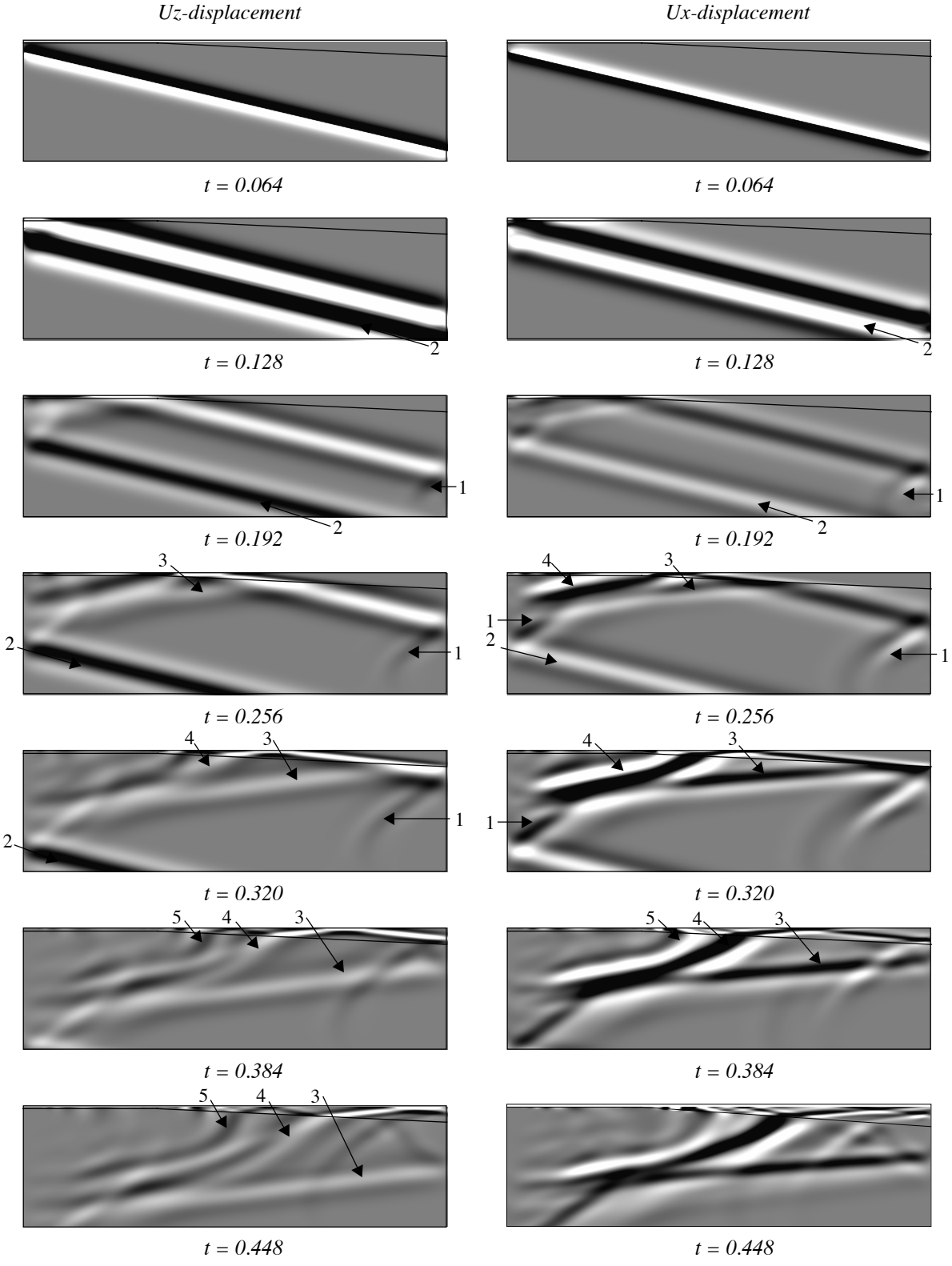

Fig. 4.15 *Snapshots of the z and x-component of the subsurface model of Fig. 4.8 with an incident P-wave with angle of incidence of 20^o. The snapshot interval is 0.064 seconds (the arrows are explained in the text).*

Because the subsurface model is exactly known we can calculate the vertical static time shifts needed to redatum the receivers to the interface of the weathered layer. Fig. 4.16a shows the calculated static correction for the P- and S-wave, which moves the receivers vertically towards the weathered layer interface. These static corrections are calculated from the distances between the weathered layer interface and the receiver position at the surface using the P- and S-wave velocity. Fig. 4.16b shows the time corrections needed for the redatuming towards a flat reference datum of 10 meter below the free-surface, corresponding to the horizontal part of the interface. Fig. 4.16c shows the total static correction for the data. The mathematical description of this static correction is given in the last part of section 4.5.

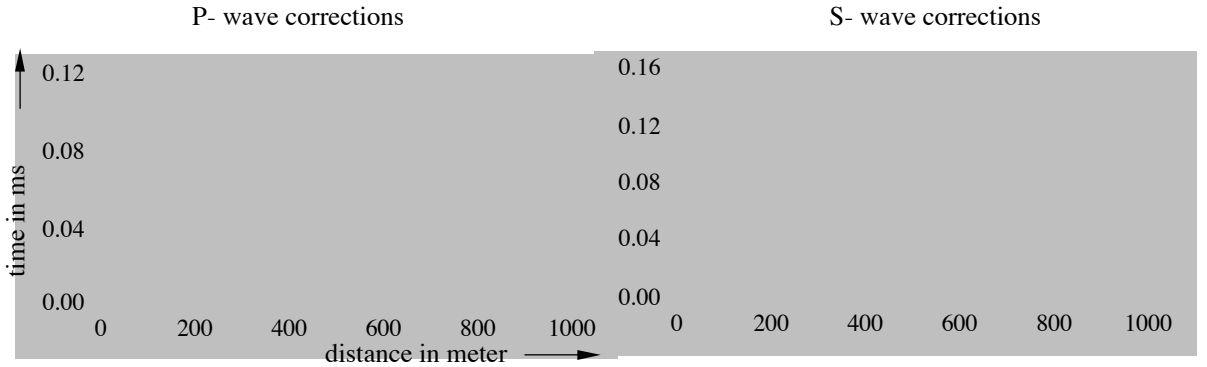

a) correction 1 (down) to the interface

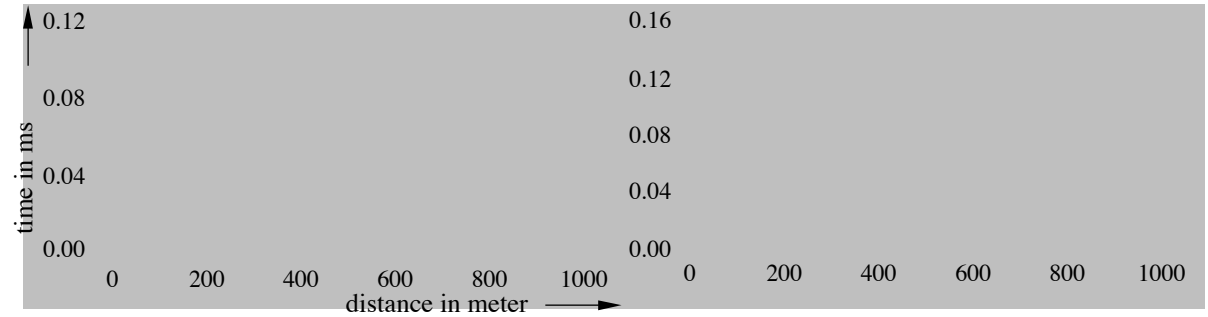

b) correction 2 (up) to the new datum

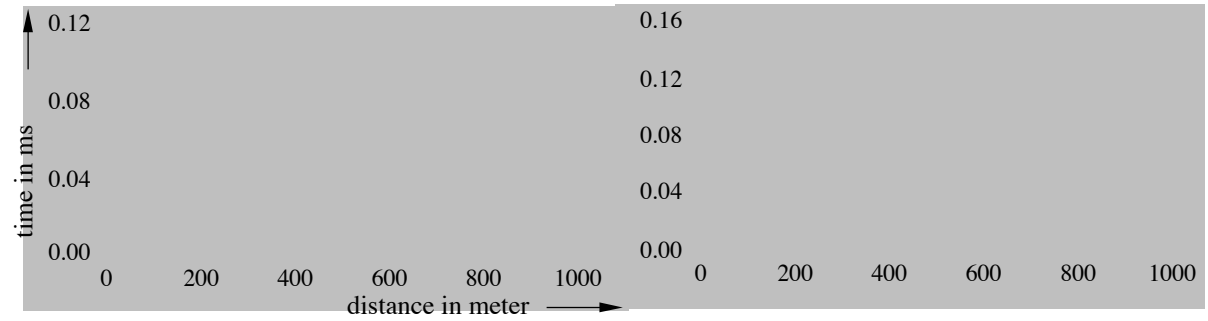

c) total correction (a minus b)

Fig. 4.16 *The corrections for the weathered layer velocity down (a), and up (b) and the combination of both corrections (c) Note the differences in P- and S-wave corrections.*

In Fig. 4.17 the two correction steps are shown. The first step is a correction for the influences of the weathered layer. The second step is a redatuming towards the new datum and adds a positive time shift to the data after the first step. The second step should *not* be done with a time shift but should use a wave equation based redatuming technique, because we cannot assume vertical propagation anymore. Nevertheless for reasons of simplicity, and to get some insight in the reliability of the static correction, we make use of this incorrect assumption. This second step needs also the velocity of the subweathered layer and the shape of the interface.

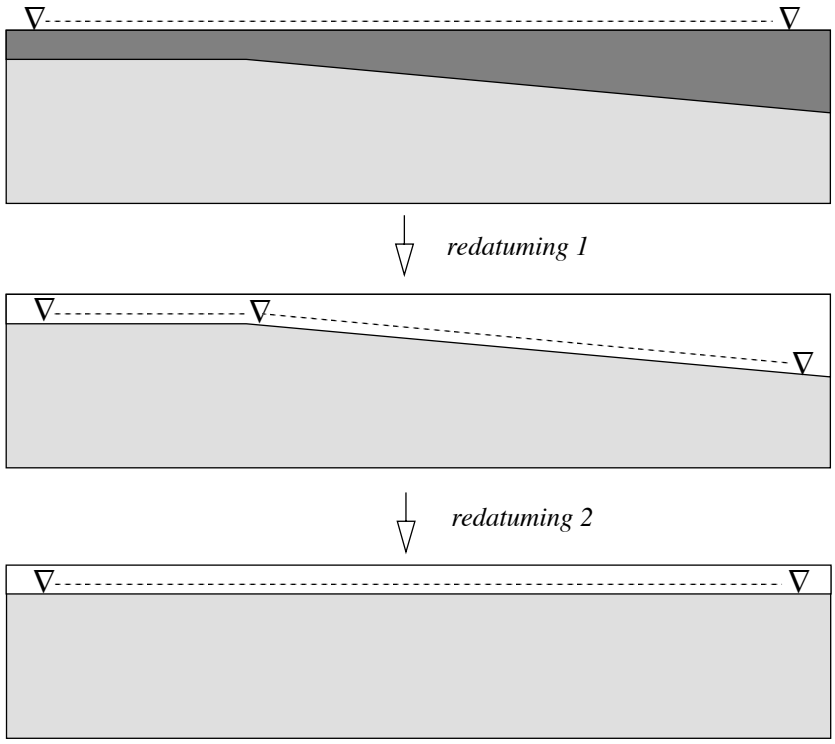

Fig. 4.17 *The two steps, for a shot record, in a layer replacement*

The objective of the weathered layer corrections, for the given examples, is to remove the break-point in the line of the arrival times of the picked maximum. In this correction vertical propagation through the weathered layer and the presence of only P-waves in the data are assumed. We therefore have to use only the Uz displacement data. In Fig. 4.18a the arrival time of the picked maximum values of the Uz-displacement records, for the first experiment, with the horizontal plane wave, are shown. The breakpoint in the line in this picture occurs at the starting point of the dipping part of the model.

In Fig. 4.18b the static correction is applied to the data (Fig. 4.18a minus Fig. 4.16a). So Fig. 4.18b shows the picked maximum after a redatuming to the interface of the weathered layer. Due to this correction the receivers are now positioned on the interface. The first arrival times for the dipping part in the model give therefore not a horizontal but an oblique line. The next step is to move the receivers from the interface to a flat datum. This is done by a time shifting redatuming technique. The redatuming is to a datum of 10 meters below the free-surface and the result is shown in Fig. 4.18c. This final result is the desired horizontal line. The line should be horizontal after correction to a horizontal datum level, because the incident plane wave is horizontal. The little irregularity in the line is due to scattering effects at the interception point of the dipping wedge with the horizontal layer. The staircase behavior of the pictures is due to the sampling interval for the receivers, which is 1 ms.

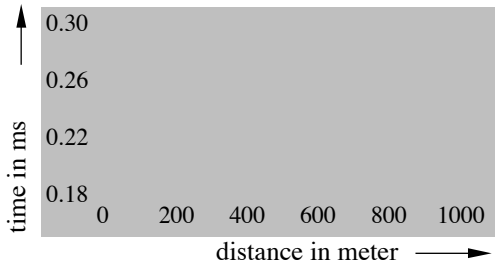

a) Arrival times of the picked maximum amplitude in the Uz records.

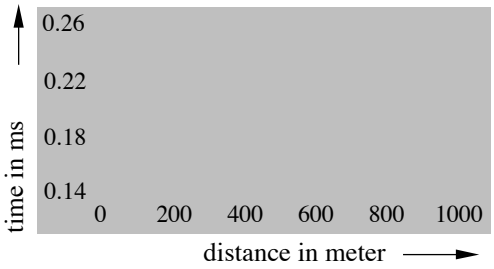

b) Static corrections applied to the maximum amplitudes, which is equal to a redatuming to the weathering interface.

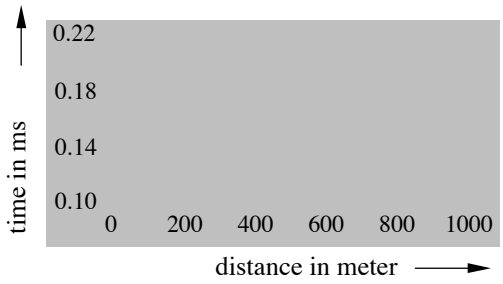

c) The result b after an additional static correction to a datum of 10 meter.

Fig. 4.18 *Static corrections shown for the maximum amplitude position of the flat plane wave*

In Fig. 4.19 the result of this static correction on the receiver records is shown for the horizontal plane wave experiment. In Fig. 4.20 the seismograms are shown for the experiment with the gradual interface. From these results it can be seen that the static correction is sufficiently accurate for a thin low velocity layer and incident plane waves with a small angle of incidence.

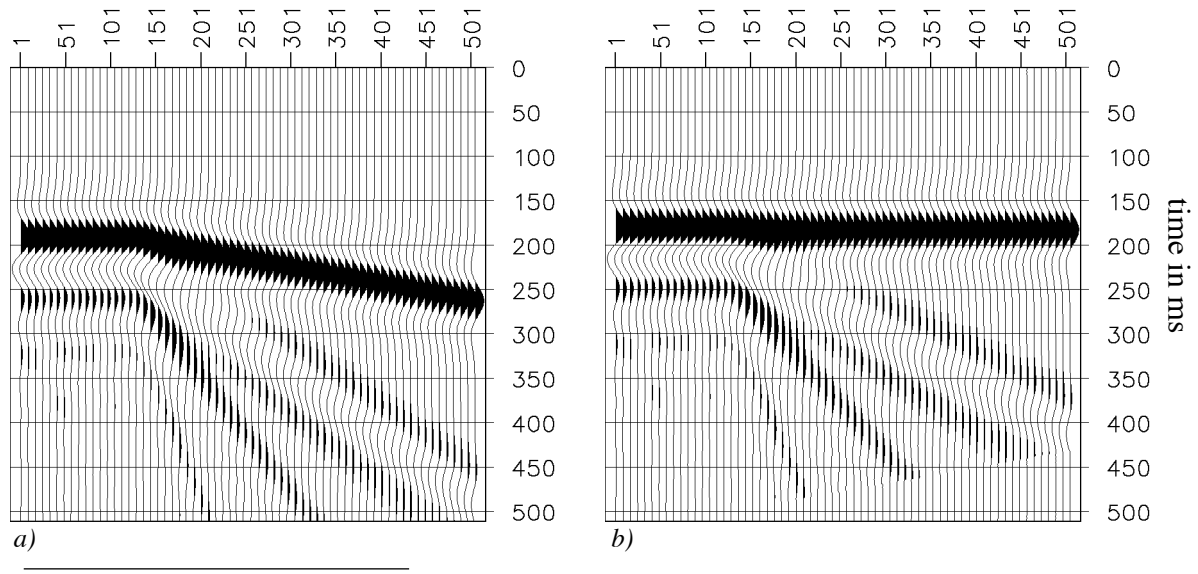

Fig. 4.19 *Static correction for the experiment with the horizontal plane wave a) shows the original received Uz data and b) shows the same data after static correction to a new datum.*

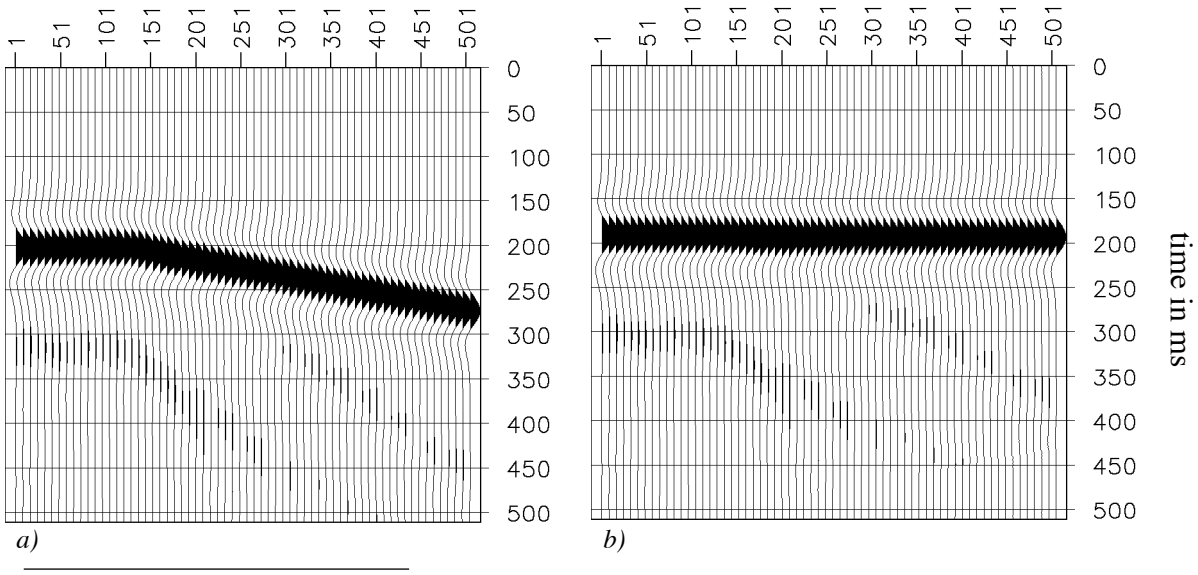

Fig. 4.20 *Static correction for the experiment with the gradual interface and a horizontal plane wave a) shows the original received Uz data and b) shows the same data after static correction to a new datum.*

In Fig. 4.21 the same kind of results as Fig. 4.18 are shown for the second experiment with the incident plane wave with an angle of 4.6^{o}. After the first correction, i.e. moving the receivers to the interface, we can see a horizontal line of the picked maximum of the receivers which are above the dipping part of the interface. This means that the wave field arrives at the same time for all receivers on the dipping part of the interface, which is correct because we have chosen the angle of incidence equal to the angle of the wedge. In Fig. 4.21c we see that the end result is a straight line (without a bending point) which corresponds to the arrival time on the new

datum of the dipping plane wave. In Fig. 4.22 the results for the experiment with an angle of incidence of 20^o are shown.

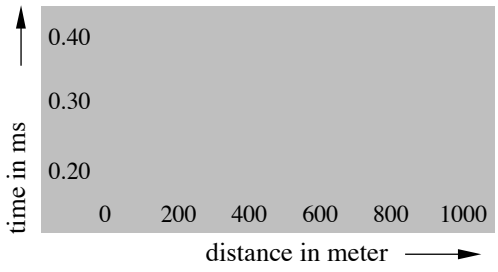

a) Arrival times of the picked maximum amplitude in the Uz records.

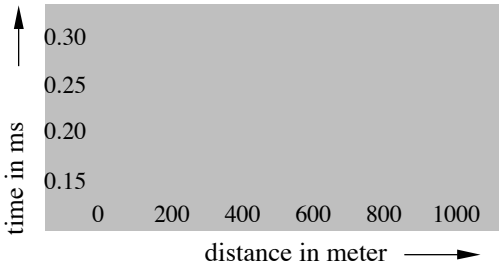

b) Static corrections applied to the maximum amplitudes, which is equal to a redatuming to the weathering interface.

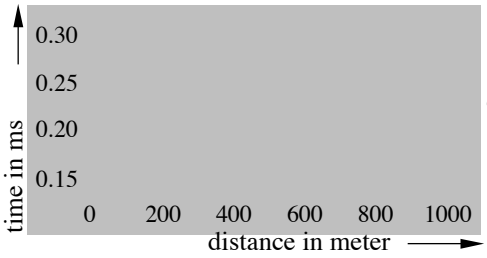

c) The result b after an additional static correction to a datum of 10 meter.

Fig. 4.22 *Static corrections shown for the maximum amplitude position of the plane wave with an angle 20^o*

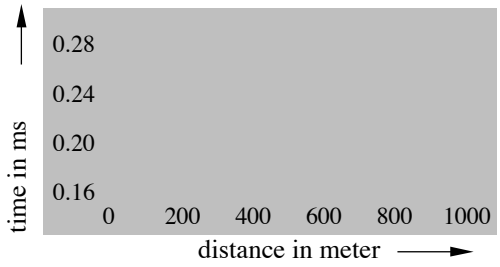

a) Arrival times of the picked maximum amplitude in the Uz records.

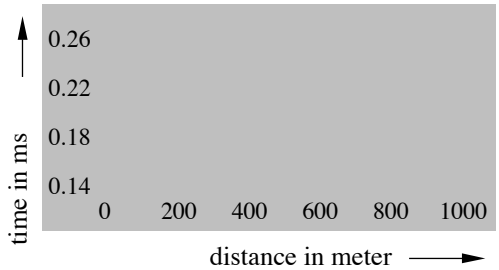

b) Static corrections applied to the maximum amplitudes, which is equal to a redatuming to the weathering interface.

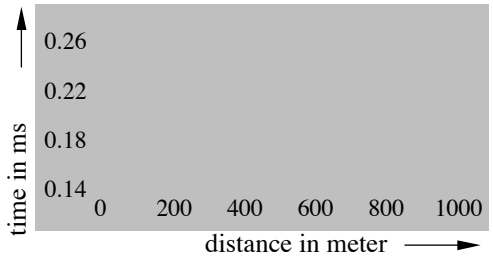

c) The result b after an additional static correction to a datum of 10 meter.

Fig. 4.21 *Static correction shown for the maximum amplitude position of the dipping plane wave, with angle of incidence is 4.6^o*

4.5 Weathered layer corrections in the DELPHI scheme

In the DELPHI project we want to introduce a propagation matrix of the weathered layer which represents corrections according to an *effective one-layer model*. The parameters, needed in this model to describe the weathered layer, must be chosen such that it can account for the disturbing propagation effects in the seismogram. Beside the short local fluctuating effects the propagation matrix must also take into account the global effects of the weathered layer and the non-vertical propagation of seismic waves through this layer.

4.5.1 The forward model of seismic data

The forward model of DELPHI is shown in Fig. 4.23. This scheme is slightly different from the scheme given in DELPHI, Volume II, Chapter 2; the decomposition operator is divided into two separated operators; the first operator $\mathbf{D}_1^{\pm}$ is a decomposition into up- and down-going traction components, the second operator $\mathbf{D}_2^{\pm}$ is a further decomposition into up- and down-going P- and S-wave field potentials, see also Chapter 2 of this volume. The $\mathbf{D}_1^{+}(z_0)$ decomposition operator is the identity matrix at the source side, and the $\mathbf{D}_1^{-}(z_0)$ operator is a "diagonal" matrix at the receiver side. The matrices consist of 2x2 sub matrices. Here "diagonal' means that only the two sub matrices on the diagonal are non-zero. The expression for the $\mathbf{D}_1^{-}(z_0)$ matrix at the receiver side can be found in chapter 2 of this volume. In this section we make use of the following definitions for the 2-dimensional elastic data vectors; the traction τ, the particle velocity V and the P- and S-wave potentials,

$$\hat{\vec{\tau}} = \begin{bmatrix} \hat{\tau}_{xz} \\ \hat{\tau}_{zz} \end{bmatrix}, \vec{V} = \begin{bmatrix} \vec{V}_x \\ \vec{V}_z \end{bmatrix}, \text{and } \vec{\vec{\Pi}} = \begin{bmatrix} \vec{\Phi} \\ \vec{\Psi} \end{bmatrix} \quad . \tag{4.5}$$

At the surface z_0 the following relations exist between these data vectors (see also Fig. 4.23):

$$\hat{\vec{\tau}}_s^{+}(z_0) = \mathbf{D}_1^{+}(z_0)\,\hat{\vec{\tau}}_s(z_0) \quad , \tag{4.6}$$

$$\vec{\vec{\Pi}}^{+}(z_0) = \mathbf{D}_2^{+}(z_0)\,\hat{\vec{\tau}}^{+}(z_0) \quad , \tag{4.7}$$

$$\hat{\vec{\tau}}^{-}(z_0) = \mathbf{D}_2^{-}(z_0)\,\vec{\vec{\Pi}}^{-}(z_0) \quad , \tag{4.8}$$

and

$$\vec{V}(z_0) = \mathbf{D}_1^{-}(z_0)\,\hat{\vec{\tau}}^{-}(z_0) \quad . \tag{4.9}$$

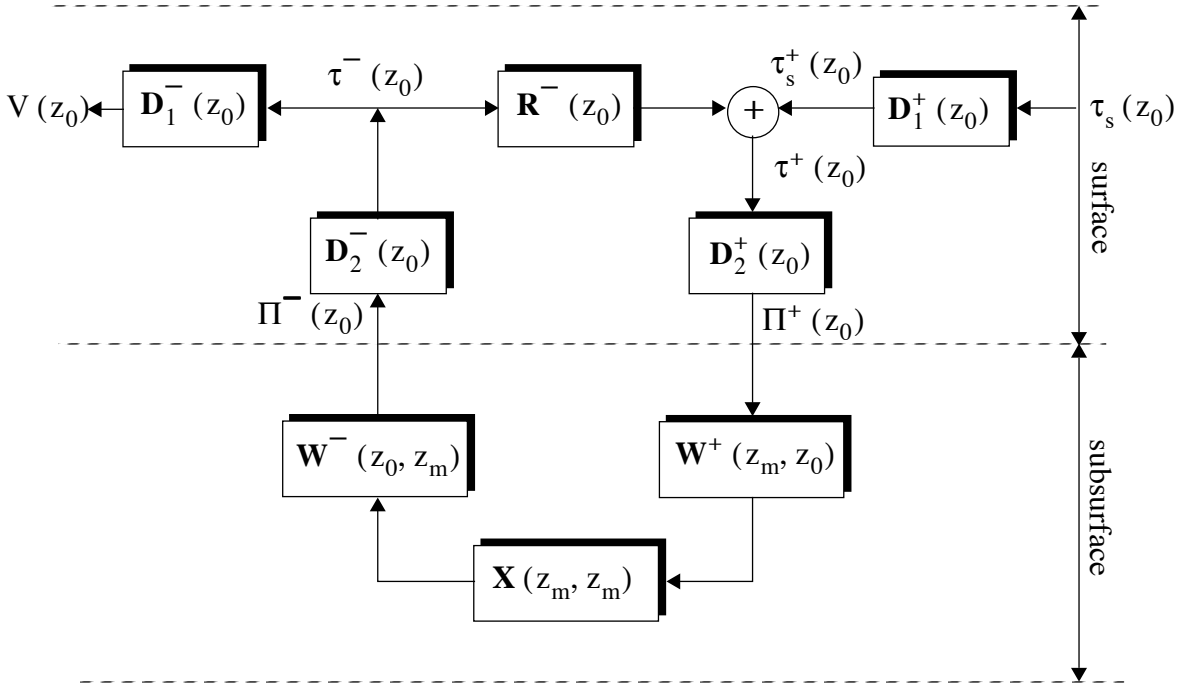

Fig. 4.23 *The forward model in DELPHI; the surface layer is not separately addressed here.*

Note that the subscript *s* in $\hat{\tau}_s$ refers to the source. The relation between $\hat{\tau}_s^+$ in equation (4.6) and $\hat{\tau}^+$ in equation (4.7), is given by (see Fig. 4.23)

$$\hat{\tau}^+(z_0) = \hat{\tau}_s^+(z_0) + \mathbf{R}^-(z_0)\,\hat{\tau}^-(z_0) \quad , \tag{4.10}$$

$$\text{with} \quad \mathbf{R}^-(z_0) = -\mathbf{I} \quad . \tag{4.11}$$

In this forward model we will introduce propagation matrices which represent the weathered layer influences.

4.5.2 The weathered layer propagation matrices

In Fig. 4.24 the surface part of the forward model described in Fig. 4.23 is repeated. In Fig. 4.25 the surface layer is separately addressed; we have placed the weathered layer propagation matrix in this forward model before the second decomposition operator at the source side and after the second decomposition matrix at the receiver side. In this approach the correction matrices are defined as

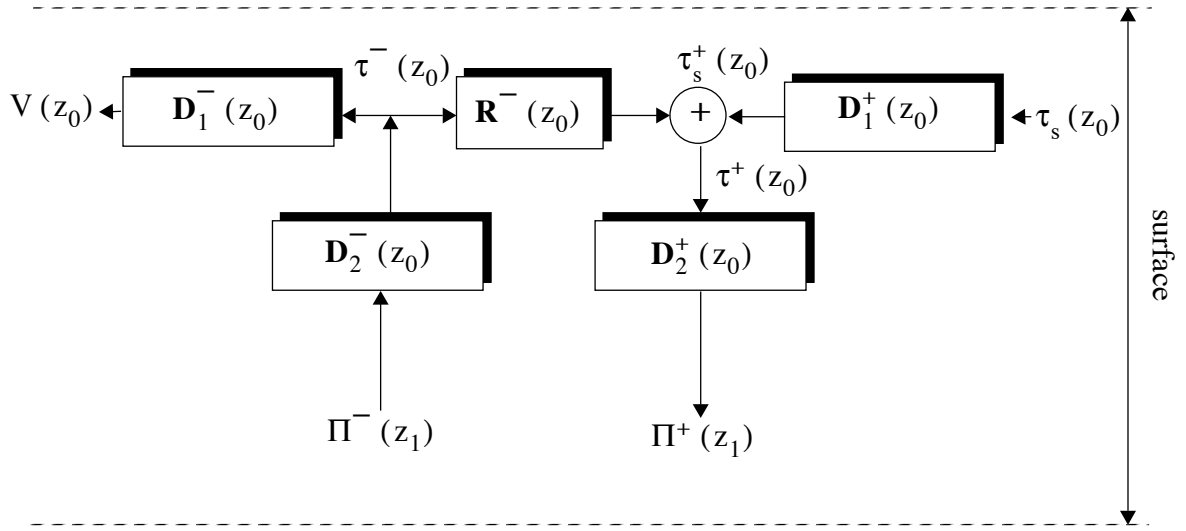

Fig. 4.24 *The surface part of the forward model given in Fig. 4.23.*

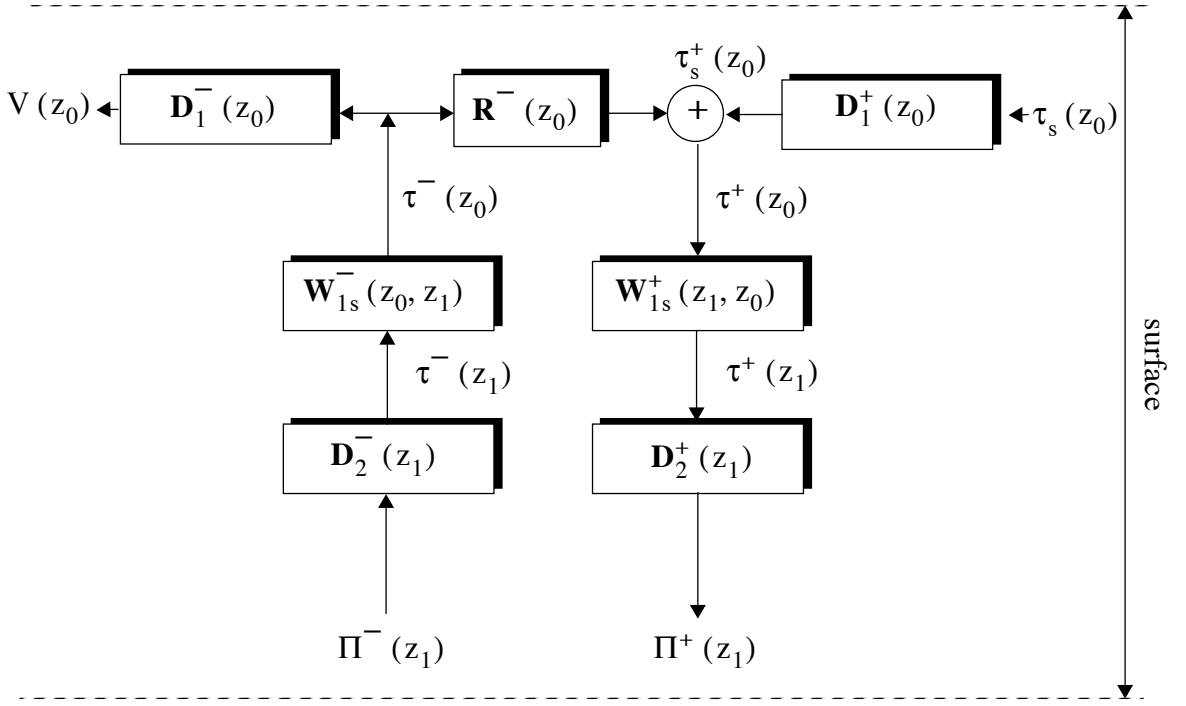

Fig. 4.25 *The forward model with the weathered layer propagation matrix placed above the second decomposition operator.*

$$\hat{\tau}^{+}(z_1) = \mathbf{W}_{1s}^{+}(z_1, z_0)\,\hat{\tau}^{+}(z_0) \quad , \tag{4.12}$$

$$\hat{\tau}^{-}(z_0) = \mathbf{W}_{1s}^{-}(z_0, z_1)\,\hat{\tau}^{-}(z_1) \quad , \tag{4.13}$$

where in the most general situation $z_0 = z_0(x, y)$ and $z_1 = z_1(x, y)$. The second decomposition operator is now defined for depth level z_1

$$\vec{\Pi}^{+}(z_1) = \mathbf{D}_2^{+}(z_1)\,\hat{\tau}^{+}(z_1) \quad , \tag{4.14}$$

$$\hat{\tau}^{-}(z_1) = \mathbf{D}_2^{-}(z_1)\,\vec{\Pi}^{-}(z_1) \quad . \tag{4.15}$$

The propagation matrices which are defined as above have in general not a simple structure. The advantage of this approach is that the decomposition into P- and S-waves is carried out on a more reliable datum level z_1.

Another approach of weathered layer corrections is to place the weathered layer propagation matrices after the second decomposition matrix at the source side and before the second decomposition matrix at he receiver side (see Fig. 4.26). This leads to the following equations

$$\vec{\Pi}^{+}(z_1) = \mathbf{W}_{2s}^{+}(z_1, z_0)\,\vec{\Pi}^{+}(z_0) \tag{4.16}$$

$$\vec{\Pi}^{-}(z_0) = \mathbf{W}_{2s}^{-}(z_0, z_1)\,\vec{\Pi}^{-}(z_1) \tag{4.17}$$

If vertical propagation through the weathered layer is assumed then the operator $\mathbf{D}_2^{\pm}$ reduces to

$$\mathbf{D}_2^{\pm}(z_0) = k_s^2 \begin{bmatrix} 0 & -\mathbf{I} \\ \mathbf{I} & 0 \end{bmatrix} \tag{4.18}$$

and the weathered layer propagation matrix reduces to a diagonal matrix. The expression for the matrix $\mathbf{W}_{2s}^{\pm}$ is given in appendix A of this chapter.

In the coming year we want to investigate particularly the relation between the decomposition process and the weathered layer properties. In the light of this research we also make a decision where we place the correction matrices in the forward model.

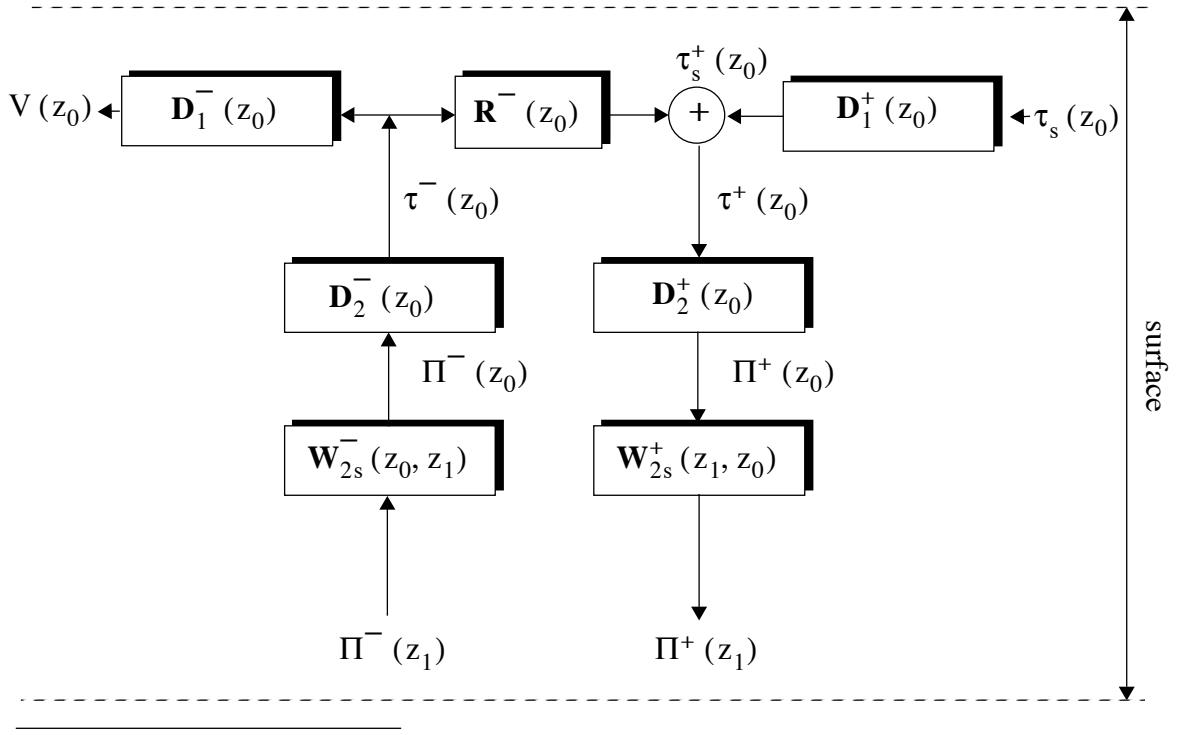

Fig. 4.26 *The forward model with the weathered layer propagation matrix placed below the second decomposition operator.*

We can compare the elastic scheme, described above, with an acoustic scheme in which the conventional static correction is implemented. The conventional acoustic static correction technique contains time shifts and amplitude decays which are applied directly to the fields emitted by the source and arriving at the receiver stations. Every source and receiver station position has its own correction. The acoustic scheme with the conventional static correction matrices placed in it is given in Fig. 4.27.

In this acoustic forward model the static correction operators are placed before the propagation operator at the source side and after the propagation operator at the receiver side

The two *static* matrices presented in Fig. 4.27 are defined by equation (4.19) and equation (4.20)

$$\vec{\hat{P}}^{+}(z_1) = \mathbf{W}_s^{+}(z_1, z_0)\,\vec{\hat{P}}^{+}(z_0) \quad , \tag{4.19}$$

$$\vec{\hat{P}}^{-}(z_0) = \mathbf{W}_s^{-}(z_0, z_1)\,\vec{\hat{P}}^{-}(z_1) \quad . \tag{4.20}$$

In this conventional static description the correction matrix $\mathbf{W}_s^{\pm}$ has the form of a diagonal matrix and is for the source side and the receiver side, in the space frequency domain, given by equation (4.21a) and equation (4.21b)

$$\mathbf{W}_s^+(z_1, z_0) = \begin{bmatrix} e^{-j\omega\Delta T_I} & 0 & 0 \\ 0 & e^{-j\omega\Delta T_j} & 0 \\ 0 & 0 & e^{-j\omega\Delta T_N} \end{bmatrix}, \tag{4.21a}$$

$$\mathbf{W}_s^-(z_0, z_1) = \begin{bmatrix} e^{-j\omega\Delta T_I} & 0 & 0 \\ 0 & e^{-j\omega\Delta T_i} & 0 \\ 0 & 0 & e^{-j\omega\Delta T_M} \end{bmatrix}, \tag{4.21b}$$

where

$$\Delta T_i = \frac{\Delta z(x_i, y_i)}{C}. \tag{4.22}$$

In this representation the static operator consists of a correction of the receiver level towards the weathered layer interface, thereby assuming, in this redatuming procedure, vertical propagation through the weathered layer. This correction method has been used in the examples of section 4.4.

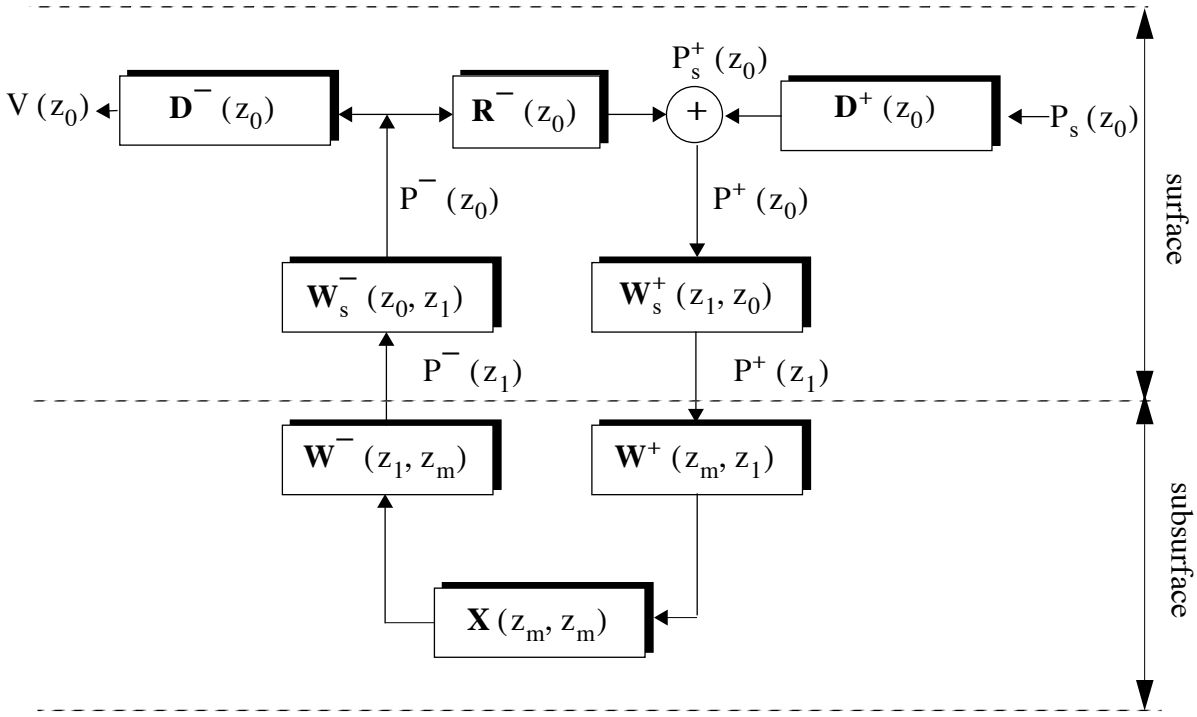

Fig. 4.27 *Acoustic forward model for single component data.*

4.6 Future plans

In DELPHI we want to approach the statics problem with the aid of a propagation matrix presentation of the first layer. This propagation matrix will be part of the total DELPHI model for land data.

In particular, we will integrate the statics problem with the decomposition process for P and S waves.

4.7 References

Berkhout, A.J., 1982, *Seismic Migration, Imaging of acoustic energy by wave field extrapolation, A) theoretical aspects*, Developments In Solid Earth Geophysics, Volume 14.A,Elsevier Science Publishers B.V.

Berkhout, A.J., 1987, *Applied seismic wave theory*, Elsevier Science Publishers B.V.

Berryhil, J.R., 1979, *Wave-equation datuming*, Geophysics, Volume 44, p. 1329-1344.

Berryhil, J.R., 1984, *Wave-equation datuming before stack*, Geophysics, Volume 49, p. 2064-2066.

DELPHI, 1990, Progress report Vol.1 and Vol.2, *From seismic measurements to rock and pore parameters*, Laboratory of Seismics and Acoustics, Delft University of Technology.

Kirchheimer, F., 1990, *Residual statics by CDP-localized stack optimization*, Geophysical prospecting, Volume 38, p. 577-606.

Press, F., and Siever, R., 1982, *Earth*, third edition, W.H Freeman and Company, San Francisco, Chapter 4,5 and 11.

Ronen, J., and Claerbout, J.F., 1985, *Surface-consistent residual statics estimation by stack--power maximization*, Geophysics, Volume 50, p. 2759-2767.

Shtivelman, V., and Canning, A., 1988, *Datum correction by wave-equation extrapolation*, Geophysics, Volume 53, p. 1311-1322.

Taner, M.T., Koehler, F., and Alhilali, K.A., 1974, *Estimation and correction of near-surface time anomalies*, Geophysics, Volume 39, p. 441-463.

Taner, M.T., and Koehler, F., 1981, *Surface consistent corrections*, Geophysics, Volume 46, p. 17-22.

Wapenaar, C.P.A., and Berkhout, A.J., 1985, *Velocity determination in layered systems with arbitrary curved interfaces by means of wave field extrapolation of CMP data*, Geophysics, Volume 50, p.63-76.

Wapenaar, C.P.A., and Berkhout, A.J., 1989, *Elastic wave field extrapolation, Redatuming of single-and multi-component seismic data*, Elsevier Science Publishers.

Wiest, B., and Edelmann, H.A.K., 1984, *Static corrections for shear wave sections*, Geophysical prospecting, Volume 32, p. 1091-1102.

Wiggins, R.A., Larner, K.L., and Wisecup, R.D., 1976, *Residual statics analysis as a general linear inverse problem*, Geophysics, Volume 41, p. 922-938.

Yilmaz, O., and Lucas, D., 1986, *Prestack layer replacement*, Geophysics, Volume 51, p. 1355-1369.

Appendix A4: Description of the weathered layer propagation matrices

In this appendix the structure of the weathered layer propagation matrices for three dimensional media are given. We will show the weathered layer propagation matrices which are based on the wave-equation and have different corrections for the P-and S-wavefields.

By placing the weathered layer propagation matrices after the second decomposition operator at the source side the structure of the matrices becomes less complex then by placing the matrices before the second decomposition operator. These more simple weathered layer propagation matrices are defined by

$$\vec{\vec{\Pi}}^{+}(z_1) = \mathbf{W}^{+}_{2s}(z_1, z_0)\,\vec{\vec{\Pi}}^{+}(z_0) \tag{A4.1}$$

$$\vec{\vec{\Pi}}^{-}(z_0) = \mathbf{W}^{-}_{2s}(z_0, z_1)\,\vec{\vec{\Pi}}^{-}(z_1) \tag{A4.2}$$

In Wapenaar and Berkhout (1989) the structure of the propagation matrix $\mathbf{W}^{\pm}_{2s}$, for P-and S-waves in a three-dimensional homogeneous and isotropic medium between z_0 and z_1, is given in the wavenumber frequency domain by

$$\tilde{\mathbf{W}}^{\pm}_{2s} = \begin{bmatrix} \tilde{W}^{\pm}_{\phi,\phi} & 0 & 0 \\ 0 & \tilde{W}^{\pm}_{\psi_1,\psi_1} & 0 \\ 0 & 0 & \tilde{W}^{\pm}_{\psi_2,\psi_2} \end{bmatrix} , \tag{A4.3}$$

where for the P-waves

$$\tilde{W}^{\pm}_{\phi,\phi}(k_x, k_y; \Delta z; \omega) = e^{-jk_{z,p}\Delta z} , \tag{A4.4}$$

and for the S-waves

$$\tilde{W}^{\pm}_{\psi_\alpha,\psi_\beta}(k_x, k_y; \Delta z; \omega) = \delta_{\alpha\beta} e^{-jk_{z,s}\Delta z} . \tag{A4.5}$$

In these equations $k_{z,p}$ and $k_{z,s}$ are defined by

$$\begin{aligned} k_{z,p} &\equiv \sqrt{k_p^2 - (k_x^2 + k_y^2)} \\ k_{z,s} &\equiv \sqrt{k_s^2 - (k_x^2 + k_y^2)} \end{aligned} , \tag{A4.6}$$

and

$$\begin{aligned} \Delta z &= |z_1 - z_0| \\ k_p &= \frac{\omega}{C_p} \\ k_s &= \frac{\omega}{C_s} \end{aligned} \quad . \tag{A4.7}$$

So in the wavenumber frequency domain the correction matrices are diagonal 3x3 matrices. The correction is a multiplication of the common source- and common receiver-data with the factors described by equation (A4.4) for the P-waves and equation (A4.5) for the S-waves. For example the source side correction can be written in matrix notation as

$$\begin{bmatrix} \tilde{\Phi}^+(z_1) \\ \tilde{\Psi}_x^+(z_1) \\ \tilde{\Psi}_y^+(z_1) \end{bmatrix} = \begin{bmatrix} e^{-jk_{z,p}\Delta z} & 0 & 0 \\ 0 & e^{-jk_{z,s}\Delta z} & 0 \\ 0 & 0 & e^{-jk_{z,s}\Delta z} \end{bmatrix} \begin{bmatrix} \tilde{\Phi}^+(z_0) \\ \tilde{\Psi}_x^+(z_0) \\ \tilde{\Psi}_y^+(z_0) \end{bmatrix} \quad . \tag{A4.8}$$

If we assume vertical propagation through the weathered layer then

$$k_x = k_y = 0 \quad , \tag{A4.9}$$

and equations (A4.6) reduce to

$$\begin{aligned} k_{z,p} &= k_p \\ k_{z,s} &= k_s \end{aligned} \quad . \tag{A4.10}$$

In making this assumption the propagation matrices are reduced to a time shift similar to the static shift, but now separately defined for the P- and S-wave

$$\tilde{W}^{\pm}_{\phi,\phi} = e^{-j\omega\frac{\Delta z}{C_p}} \quad , \tag{A4.11}$$

$$\tilde{W}^{\pm}_{\psi_\alpha,\psi_\beta} = \delta_{\alpha\beta} e^{-j\omega\frac{\Delta z}{C_s}} \quad . \tag{A4.12}$$

The expression of the correction matrix in equation (A4.3) in the space-frequency domain is given by

$$\mathbf{W}^{\pm}_{2s} = \begin{bmatrix} \mathbf{W}^{\pm}_{\phi,\phi} & 0 & 0 \\ 0 & \mathbf{W}^{\pm}_{\psi_1,\psi_1} & 0 \\ 0 & 0 & \mathbf{W}^{\pm}_{\psi_2,\psi_2} \end{bmatrix} \quad , \tag{A4.13}$$

The multiplication in the wavenumber frequency domain in equation (A4.8) is replaced by a convolution in the space frequency domain. The columns of the submatrices $\mathbf{W}^{\pm}_{\psi_\alpha,\psi_\beta}, \mathbf{W}^{\pm}_{\phi,\phi}$ contain in the space frequency domain the elastic Rayleigh operators (Wapenaar, 1989),

$$W^{\pm}_{\phi,\phi} = \frac{1}{2\pi}\cos\varphi\frac{1+jk_p\Delta r}{\Delta r^2}e^{-jk_p\Delta r} \quad , \tag{A4.14}$$

$$W^{\pm}_{\psi_\alpha,\psi_\beta} = \frac{\delta_{\alpha\beta}}{2\pi}\cos\varphi\frac{1+jk_s\Delta r}{\Delta r^2}e^{-jk_s\Delta r} \quad , \tag{A4.15}$$

where $\cos\varphi = \dfrac{(z_1 - z_0)}{\Delta r}$ and

$$\Delta r = \sqrt{x^2 + y^2 + (z_1 - z_0)^2} \quad . \tag{A4.16}$$

For non horizontal layers and a lateral varying surface Δz is a function of the coordinates x and y.

$$\Delta z\,(x, y) = (z_1\,(x, y) - z_0\,(x, y)) \tag{A4.17}$$

Making use of the matrix notation the spatial-convolution (for simplicity given in 2-dimensions) for P-waves can be written as

(A4.18)

$$\begin{bmatrix} \Phi^+(\Delta x, z_1) \\ \cdots \\ \cdots \\ \cdots \\ \Phi^+(n\Delta x, z_1) \\ \cdots \\ \cdots \\ \cdots \\ \Phi^+(N\Delta x, z_1) \end{bmatrix} = \begin{bmatrix} W_{1,1} & \cdots & W_{1,m} & 0 & \cdots & \cdots & \cdots & \cdots & 0 \\ W_{2,1} & \cdots & \cdots & W_{2,m+1} & 0 & \cdots & \cdots & \cdots & 0 \\ W_{m,1} & \cdots & W_{m,m} & \cdots & W_{m,2m-1} & 0 & \cdots & \cdots & 0 \\ 0 & W & \cdots & \cdots & \cdots & W & \cdots & \cdots & 0 \\ 0 & \cdots & W_{m+i,i} & \cdots & \cdots & \cdots & W_{m+i,2m+i+1} & \cdots & 0 \\ 0 & \cdots & \cdots & W & \cdots & \cdots & \cdots & W & 0 \\ 0 & \cdots & \cdots & 0 & W_{N-m,N-2m-1} & \cdots & \cdots & \cdots & W_{N-m,N} \\ 0 & \cdots & \cdots & \cdots & 0 & W_{N-1,N-m-1} & \cdots & \cdots & W_{N-1,N} \\ 0 & \cdots & \cdots & \cdots & \cdots & 0 & W_{N,N-m} & \cdots & W_{N,N} \end{bmatrix} \begin{bmatrix} \Phi^+(\Delta x, z_0) \\ \cdots \\ \cdots \\ \cdots \\ \Phi^+(j\Delta x, z_0) \\ \cdots \\ \cdots \\ \cdots \\ \Phi^+(N\Delta x, z_0) \end{bmatrix}$$

In comparison with equation (A4.11) and equation (A4.12) we have introduced off diagonal elements into the correction matrices which describe the non vertical propagation effects of the wave fields. The elements $(W^{+}_{\phi,\phi})_{n,j}$ of the propagation matrix for the P-waves in equation (A4.18) are given by

$$(W^{+}_{\phi,\phi})_{n,j} = \frac{-jk}{2}\cos\varphi_{n,j} H_1^{(2)}(k\Delta r_{n,j}), \tag{A4.19}$$

where $H_1^{(2)}$ is the first order Hankel function of the second kind and

$$\Delta r_{n,j} = \sqrt{(n\Delta x_{z_1} - j\Delta x_{z_0})^2 + (z_1(n\Delta x) - z_0)^2} \quad , \tag{A4.20}$$

and

$$\cos\varphi_{n,j} = \frac{z_1(n\Delta x) - z_0}{\Delta r_{n,j}} \quad . \tag{A4.21}$$

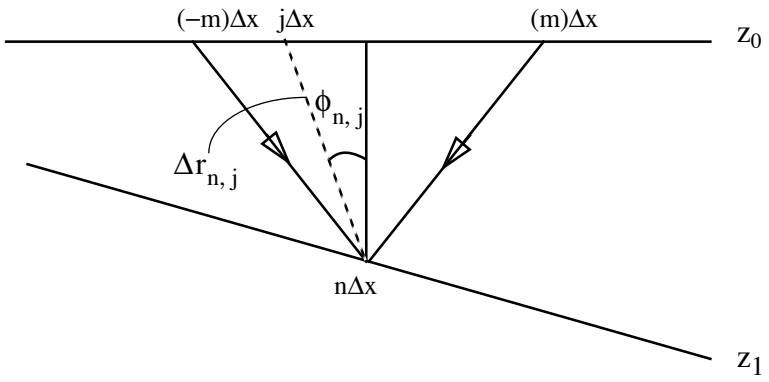

Fig. A4.1 *The geometries for forward extrapolation at the source side.*

In Fig. A4.1 the forward extrapolation at the source side of equation (A4.18) is visualized. The convolution for one subsurface point n is given by,

$$\Phi_n(z_1) = \sum_i (W^{\pm}_{\phi,\phi})_{n,i} \Phi_i(z_0) \tag{A4.22}$$

where $(W^{\pm}_{\phi,\phi})_{n,j}$ is a convolution operator of length 2m-1.